REVISTA INTERDISCIPLINAR DE PESQUISA EM ENGENHARIA

CILAMCE 2016

XXXVII IBERIAN LATIN AMERICAN CONGRESS ON COMPUTATIONAL METHODS IN ENGINEERING
BRASÍLIA - DF - BRAZIL

# TWO-DIMENSIONAL SIMULATIONS VIA FINITE ELEMENTS OF DIRECT ETHANOL FUEL CELLS (DEFC)

**Marcelo Maraschin de Souza**

marcelo.maraschin@ifsc.edu.br

Instituto Federal de Santa Catarina

St. Heitor Villa Lobos 222, Lages - SC, 88506-400, Brazil

**Ranon de Souza Gomes**

**Álvaro Luiz De Bortoli**

ranon.souza@ufrgs.br

dbortoli@mat.ufrgs.br

Universidade Federal do Rio Grande do Sul

Av. Bento Gonalves 9500, Porto Alegre - RS, 91509-900, Brazil

***Abstract.*** *A solution to the growing energy demand and depletion of oil supplies is its best use, along with the development of renewable sources according to the needs and possibilities of each user. An attractive alternative is the fuel cell. Fuel cells provide clean energy and with high efficiency in a wide variety of applications. In addition, they enable greater reliability in power supply with less emissions of pollutants in the air. The present work develops a two-dimensional model for a direct ethanol fuel cell. A code is developed in Fortran90 using the finite element method to calculate the flow in different layers of the cell (input and output channels, diffusion layer and catalyst layer). The model takes into account the losses overpotentials at the anode and at the cathode, providing a better understanding of the physical and chemical behavior within the cell, and about the conversion of chemical energy into electricity. This corresponds to the main contribution of the present work.*

***Keywords:*** *PEM Fuel Cell, Ethanol, Finite Element Method, Modeling*

# 1 INTRODUCTION

The combustion in internal combustion engines is still one of the main processes responsible to transform energy. In some traditional electric power generating systems, first the fuel is burned to produce heat, then heat is converted into mechanical energy and finally into electricity. One device that uses more efficiently the available sources of energy is the fuel cell. A fuel cell is an electrochemical device that converts chemical energy present in fuels directly into electrical energy. Among the main advantages of a fuel cell, it appears the convenience of the instantaneous recharging (the cell produces electricity as long as there is fuel), low emission of pollutants into the atmosphere, and is quiet, compact and lightweight. Fuel cells provide clean energy and with high efficiency in a wide variety of applications.

Much of the work developed for fuel cells has focused on cells that use hydrogen as an energy source. On the other hand, the methanol also gained interest in the last 20 years as an alternative fuel to hydrogen for use in fuel cells. However, the hydrogen still requires efficient technologies for its storage and the methanol can cause environmental problems due to its toxicity. Thus, a promising fuel that has gained great interest in recent years is the ethanol. Ethanol is a renewable fuel that can be produced from biomass. It has a pre-established infrastructure, which can be easily adapted to the industry of vehicles using fuel cells.

Biomass is a clean and renewable source of energy available in abundance and derived from organic materials. All that accomplish of photosynthesis or something derivative that performs photosynthesis can be used as biomass. The transformation of biomass occurs through the carbon cycle where the burning of organic material and their derivatives produce the release of $CO_2$ into the atmosphere. Plants, in turn, through photosynthesis, convert $CO_2$ to carbohydrates, releasing oxygen in the environment. In addition, the energy extracted from biomass generates many jobs in the industry and many jobs in rural areas.

Fuel cells have attracted the interest of researches in recent years, and many studies were conducted to estimate the relationship between the cell voltage versus the current density of a DEFC. Some studies using the finite element method for numerical simulations in PEM fuel cells are found in the literature (Futerko and Hsing, 2000; Cheddie and Munroe, 2006). Most of these studies make use of one-dimensional models to approximate the flow in the different layers of DEFCs. Two and three-dimensional models are rarely found in the literature. Therefore, in this work, numerical simulations are developed with the finite element method, which is known to have a good mathematical theoretical basis (Brenner and Scott, 2008; Johnson, 1987). The equations are considered transient, and are discretized by the Runge-Kutta method of order 3.

According to Abdullah et. al (2014), the development of DEFC still requires a multidimensional and multiphase model capable of describing the complex physical and chemical phenomena inside the DEFC. Therefore, this work proposes a two-dimensional mathematical model to estimate the flow of the fuel inside the DEFC, taking into account all losses overpotentials.

# 2 DIRECT ETHANOL FUEL CELL

In a typical direct ethanol fuel cell, the mixture of ethanol and water is inserted into the anode side, which reacts to form carbon dioxide, protons, and electrons. An outline of the fuel cell used in this work is shown in Figure 1. The anode is located on the left side and the cathode is on the right, and $X_{EtOH}$ and $X_{O_2}$ are the mole fraction of ethanol and oxygen, respectively.

$\delta_{cd}$ and $\delta_{cc}$ are thickness of the diffusive layer and of the catalyst layer, respectively, and $\delta_m$ is the membrane thickness.

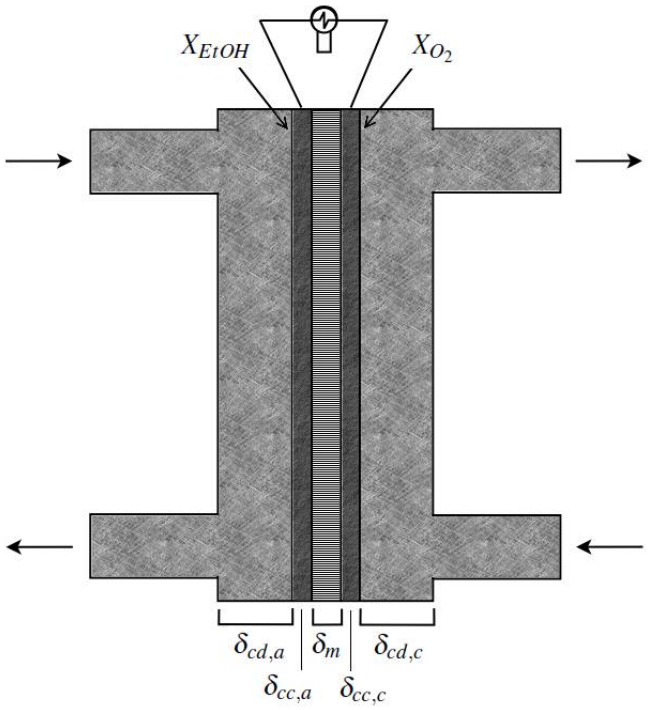


**Figure 1: Sketch of direct ethanol fuel cell**

The protons pass preferably to the cathode through the membrane and the electrons through an external circuit, providing a difference of potential. On the cathode side, the air reacts with the protons and electrons formed at the anode to produce water vapor (Al-Baghdadi, 2005). A catalyst $PtRu/C$ is used at the anode and $Pt/C$ at the cathode (Pramanik and Basu, 2010). The electrochemical reactions that take place inside the cell are given by:

$$C_2H_5OH + 3H_2O \rightarrow 2CO_2 + 12H^+ + 12e^- \quad \text{at the anode,} \tag{1}$$

$$3O_2 + 12H^+ + 12e^- \rightarrow 6H_2O \quad \text{at the cathode,} \tag{2}$$

corresponding to the overall reaction

$$C_2H_5OH + 3O_2 \rightarrow 2CO_2 + 3H_2O. \tag{3}$$

The complete oxidation of ethanol in carbon dioxide is complicated by the difficulty in breaking C-C bonds, forming intermediates which are adsorbed on the catalyst surface. Goel and Basu (2015) proposed three elementary steps for the electro-oxidation of ethanol, as follow:

$$C_2H_5OH + Pt \rightarrow (C_2H_5OH)_{ad,Pt} \rightarrow (CH_3CHO)_{ad,Pt} + 2H^+ + 2e^- \tag{4}$$

$$3H_2O + 3Ru \leftrightarrow 3(OH)_{ad,Ru} + 3H^+ + 3e^- \tag{5}$$

$$(CH_3CHO)_{ad,Pt} + 3(OH)_{ad,Ru} \rightarrow 2CO_2 + 7H^+ + 7e^- + Pt + 3Ru. \tag{6}$$

## 3 GOVERNING EQUATIONS

In the anode and cathode the equations have the same form, given by continuity, momentum, and species conservation. These equations are written as:

## 3.1 Continuity equation:

We consider here an incompressible fluid and constant viscosity, then the continuity is given by

$$\nabla \cdot u = 0. \tag{7}$$

## 3.2 Momentum equation:

The velocity and pressure for two-dimensional time dependent Navier-Stokes equations are given by

$$\rho \frac{\partial u}{\partial t} + \rho u \cdot \nabla u = -\nabla p + \mu \nabla^2 u + \rho S_u, \tag{8}$$

where $\rho$ is the density, $u = (u^1, u^2)$ is the velocity, $\mu$ is the viscosity and $p$ is the pressure. Table 1 shows the source term $S_u$, where $\varepsilon_d$ and $\varepsilon_c$ are the porosities of the diffusion layer and of the catalyst layer, respectively, and $k$ is the permeability. The fluid velocity in the diffusion and catalyst layers is described by Darcy's law (Liu and Wang, 2007).

**Table 1: Source term $S_u$.**

| | flow channel | diffusion layer | catalyst layer |
|---|---|---|---|
| $S_u$ | 0 | $-\varepsilon_d \frac{\mu}{k} u$ | $-\varepsilon_c \frac{\mu}{k} u$ |

## 3.3 Species equations:

The main species satisfies an equation of the type

$$\rho \frac{\partial X_k}{\partial t} + \rho u \cdot \nabla X_k = \rho D_k^{\text{eff}} \nabla^2 X_k + S_k, \qquad \text{with} \quad \sum_k X_k = 1. \tag{9}$$

where $X_k$ is the mole fraction of species $k$, $D_k^{\text{eff}}$ is the effective diffusion coefficient and $S_k$ is the sources term. The Table 2 and the Table 3 present the source term $S_k$, where $j_a$ and $j_c$ are the current density in the anode and cathode, $M_{EtOH}$, $M_{H_2O}$, $M_{O_2}$ and $M_{CO_2}$ are the molecular weights of ethanol, water, oxygen and carbon dioxide, respectively. The source term, $S_k$, is zero in the channels and in the diffusion layer.

**Table 2: Source term $S_k$ at the anode catalyst layer.**

| | ethanol | water | carbon dioxide |
|---|---|---|---|
| $S_k$ | $-\frac{M_{EtOH}}{2F} j_a$ | $-\frac{M_{H_2O}}{F} j_a$ | $\frac{2M_{CO_2}}{7F} j_a$ |

**Table 3: Source term $S_k$ at the cathode catalyst layer.**

| | oxygen | water |
|---|---|---|
| $S_k$ | $-\frac{M_{O_2}}{4F} j_c$ | $\frac{M_{H_2O}}{2F} j_c$ |

# 4 CELL VOLTAGE

One of the reasons of fuel cells modeling is to determine why the effective voltage differs from the thermodynamically predicted theoretical voltage. The overall cell voltage can be obtained using the following relationship:

$$V_{cell} = E^0_{cell} - (\eta_{act} + \eta_{ohm} + \eta_{con}), \tag{10}$$

where $\eta_{act}$ are the losses due to activation, $\eta_{ohm}$ are the losses due to ohmic resistance, $\eta_{con}$ are the losses due to concentration, $V_{cell}$ is the cell voltage, and $E^0_{cell}$ is the reversible voltage of DEFC ($\sim$1.14 $V$).

The modified Butler-Volmer equation is used for determining the electrochemical reaction rate of electro-oxidation of ethanol in the anode catalyst, and the reaction rate of oxygen reduction at the cathode catalyst (Pramanik and Basu, 2010; Andreadis and Tsiakaras, 2006; Andreadis et al., 2008; Colmati et al., 2006; Bard and Faulkner, 2001; Heysiattalab and Shakeri, 2011):

$$j_a = j_0 \frac{X_{EtOH}}{X^{\text{ref}}_{EtOH}} \exp\left(\frac{\alpha_a n F}{RT}\eta_a\right), \tag{11}$$

$$j_c = j_0 \frac{X_{O_2}}{X^{\text{ref}}_{O_2}} \exp\left(\frac{\alpha_c n F}{RT}\eta_c\right), \tag{12}$$

where $j_0$ is the exchange current density (at the anode and cathode), $X_{EtOH}$ is the ethanol mole fraction in the catalyst layer, $X^{\text{ref}}_{EtOH}$ is the reference ethanol mole fraction, $X_{O_2}$ is the mole fraction of oxygen in the catalyst layer, $X^{\text{ref}}_{O_2}$ is the reference oxygen mole fraction, $\alpha_a$ is the anode transfer coefficient, $\alpha_c$ is the cathode transfer coefficient, $n$ is the number of electrons transferred, $F$ is the Faraday constant, $R$ is the universal gas constant, $T$ is the temperature, $\eta_a$ is the anode overpotential and $\eta_c$ is the cathode overpotential.

## 4.1 Activation overpotential:

In an electrochemical reaction occurs the transfer of electrons at the interface between the electrode and the chemical species. There is an activation barrier that must be overcomed for transforming the reactants into products. The more strength to overcome this barrier, the faster the reaction rate.

The activation overpotential is directly related to the reaction kinetics. The relation between activation overpotential and current density at the anode is reported in the work of Pramanik and Basu (2010), and is given by:

$$\eta_{act,a} = \frac{RT}{\alpha_a n F} \ln[j_a (X_{EtOH} X_{H_2O})^{-0.25}], \tag{13}$$

where $X_{H_2O}$ is the water mole fraction in the catalyst layer. The losses by activation at the cathode can be obtained from Tafel equation (Abdullah et al., 2015; Yuan et al., 2009; Farhat, 2004), resulting in:

$$\eta_{act,c} = \frac{RT}{\alpha_c nF} \ln\left(\frac{j_c}{j_0}\right). \tag{14}$$

## 4.2 Ohmic losses:

The ohmic losses are due to the individual resistances of each component, including the ohmic resistance of the electrolyte and the electrical resistance encountered by the electrons to flow through the cell.

The driving force of the transport of ions and electrons is a potential difference. This difference is considered a loss, which occurs because the conductors are not perfect, have a resistance which follows ohmic behavior for passage of ions and electrons.

The ohmic loss is caused by the resistance to electron flow through the electrode, through the external circuit and due to the resistance to protons transport through the membrane. The ohmic losses can be written as

$$\eta_{ohm} = j_a \frac{\delta_m}{\sigma_m}, \tag{15}$$

where $\delta_m$ is the thickness of membrane, and $\sigma_m$ is the ionic conductivity for fully hydrated PEM, given by (Goel and Basu, 2015):

$$\sigma_m = 1268\sigma_m^{\text{ref}} \left(\frac{1}{T_{\text{ref}}} - \frac{1}{T}\right). \tag{16}$$

## 4.3 Concentration overpotentials:

The mass transport governs the supply and removal of reactants and products in the fuel cell. The polarization overpotential is related to mass transport limitation and can be reduced to facilitating the transport of the species on the electrode surface.

The decrease in concentration of ethanol results in concentration overpotential as the ethanol is not replenished immediately at the anode because of mass transfer resistance.

The model equation for concentration overpotential at the anode and cathode is given by, respectively (Pramanik and Basu, 2010; Abdullah et al., 2015; Andreadis et al., 2008):

$$\eta_{con,a} = \left(\frac{RT}{\alpha_a nF}\right) \ln\left(\frac{j_a}{j_0(1+j_a)}\right), \tag{17}$$

$$\eta_{con,c} = \left(\frac{RT}{\alpha_c nF}\right) \ln\left(\frac{j_c}{j_0(1-j_c N)}\right). \tag{18}$$

The parameters used for solving the model equations for DEFC are listed in the Table 4.

**Table 4: Parameters used in the model of the DEFC at 315K.**

| Parameter | Unit | Present model | Reference |
|---|---|---|---|
| $k_{O_2}$ | $cm^2$ | $1.76\times10^{-7}$ | (Ge and Liu, 2006) |
| $k_{H_2O}$ | $cm^2$ | $1.0\times10^{-7}$ | (Ge and Liu, 2006) |
| $\mu_{O_2}$ | g $cm^{-1}s^{-1}$ | $2.05\times10^{-5}$ | (Ge and Liu, 2006) |
| $\mu_{H_2O}$ | g $cm^{-1}s^{-1}$ | $4.061\times10^{-9}$ | (Suresh and Jayanti, 2011) |
| $R$ | J $mol^{-1}$ $K^{-1}$ | 8.3144 | (Pramanik and Basu, 2010) |
| $F$ | Coulomb $mol^{-1}$ | 96,487 | (Pramanik and Basu, 2010) |
| $\sigma_m$ | S $cm^{-1}$ | 0.1416 | (Abdullah et al., 2015) |
| $\delta_m$ | cm | 0.00145 | (Pramanik and Basu, 2010) |
| $\delta_{cc,a}$ | cm | 0.001 | (Suresh and Jayanti, 2011) |
| $\delta_{cc,c}$ | cm | 0.001 | (Suresh and Jayanti, 2011) |
| $\delta_{cd,a}$ | cm | 0.6 | assumed |
| $\delta_{cd,c}$ | cm | 0.6 | assumed |
| $\varepsilon_d$ | dimensionless | 0.65 | (Suresh and Jayanti, 2011) |
| $\varepsilon_c$ | dimensionless | 0.4 | (Kareemulla and Jayanti, 2009) |
| $\alpha_a$ | dimensionless | 0.08 | (Suresh and Jayanti, 2011) |
| $\alpha_c$ | dimensionless | 0.1 | (Pramanik and Basu, 2010) |
| $j_0$ | mA $cm^{-2}$ | 0.03 | (Pramanik and Basu, 2010) |
| $n$ | dimensionless | 12 | Eq. (1) |
| $N$ | dimensionless | $3.857\times10^{-13}$ | (Pramanik and Basu, 2010) |
| $M_{H_2O}$ | g $mol^{-1}$ | 18.01528 | (Pramanik and Basu, 2010) |
| $M_{EtOH}$ | g $mol^{-1}$ | 46.06844 | (Memming and Bahnemann, 2015) |
| $M_{CO_2}$ | g $mol^{-1}$ | 44.01 | (Memming and Bahnemann, 2015) |

# 5 NUMERICAL PROCEDURE

The numerical procedure used for spatial discretization was the finite element method. To obtain a variational formulation for these equations, we define the space $Y = H_0^1(\Omega)^2$ and $Q = L_0^2(\Omega)$, where $H_0^1(\Omega)^2 = \{\mathbf{v} \in L^2(\Omega)^2$ and $\nabla\mathbf{v} \in L^2(\Omega)^{2\times2} : \mathbf{v} = 0$ em $\partial\Omega\}$ is the Hilbert space $(H^1(\Omega)^2)$, with zero boundary condition and $L_0^2 = \{q \in L^2(\Omega) : \int_\Omega q\, dxdy = 0\}$ is the Hilbert space $H^0(\Omega) = L^2(\Omega)$ with zero media.

The domain discretization is obtained by a triangulation, subdividing $\Omega$ in a non-overlapping

set of triangles,

$$T^h = \cup_{j=1}^{M} K_j, \tag{19}$$

where no vertex of a triangle is over the side of another triangle, as shown in the Fig. 2 (Johnson, 1987).

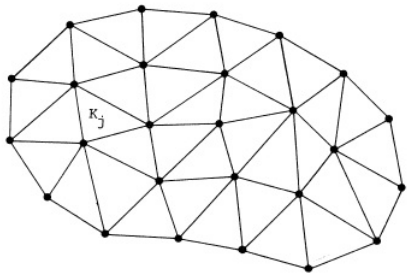


**Figure 2: 2D mesh with linear functions**

Choose spaces of finite dimension $Y_h \subset Y$ and $Q_h \subset Q$, let $Y_h$ and $Q_h$ be given by Taylor-Hood element, i.e., quadratic polynomials for velocity and linear for pressure (Layton, 2008). The choice of these elements is justified by the fact that they satisfy the inf-sup condition, which guarantees admissibility of the two discrete spaces selected. To species equations we choose quadratic polynomials too.

Thus, the finite element solution of momentum equations and continuity equation is given by, respectively

$$\rho\left(\frac{\partial u^h}{\partial t}, v^h\right) + \mu(\nabla u^h, \nabla v^h) + \rho(u^h \cdot \nabla u^h, v^h) - (p^h, \nabla \cdot v^h) = \rho(S_\nu, v^h), \tag{20}$$

$$(\nabla \cdot u^h, q^h) = 0, \tag{21}$$

where $v^h \in Y_h$, $q^h \in Q_h$, $(\cdot,\cdot)$ is the inner product in the space $L^2$ and $u^h = (u^{h,1}, u^{h,2})$, with

$$u^{h,i} = \sum_{j=1}^{M} \alpha_j^i(t)\phi_j(x,y), \tag{22}$$

where $i = 1, 2$, $M$ is degree of freedom of velocity and $\phi$ is the polynomial function (quadratic). The discretized pressure $p^h$ is given by,

$$p^h = \sum_{j=1}^{N} \beta_j(t)\psi_j(x,y), \tag{23}$$

where $N$ is degree of freedom of pressure and $\psi$ is the polynomial function (linear).

The finite element solution of species equations is given by

$$\rho\left(\frac{\partial X_k^h}{\partial t}, r^h\right) + \rho D_k^{eff}(\nabla X_k^h, \nabla r^h) + \rho(u^h \cdot \nabla X_k^h, r^h) = (S_k, r^h) \quad \forall\, r^h \in Y_h, \tag{24}$$

where, the discretized species mole fraction $X_k^h$ is

$$X_k^h = \sum_{j=1}^{P} \gamma_j^k(t)\phi_j(x,y), \tag{25}$$

where $P$ is degree of freedom of species mole fraction, $k = EtOH, H_2O, O_2, CO_2$ and the polynomial function is the same of velocity (quadratic).

The equations considered in this work are transient, so the time discretization method is very important in the process of obtaining the approximate solution.

The numerical simulations were performed using the three-stage explicit Runge-Kutta method (RK-3), which requires less computational memory. This method is characterized by the small number of operations required, and is employed because its coefficients can be selected to obtain solutions of high accuracy (in time). More than two stages are employed to extend the stability region. This scheme for partial equations of the form

$$\frac{\partial}{\partial t}W^h + R^h = 0, \tag{26}$$

is given by

$$\overrightarrow{W}_0^h = \overrightarrow{W}_n^h, \tag{27}$$

$$\overrightarrow{W}_r^h = \overrightarrow{W}_0^h - \alpha_r \Delta t \overrightarrow{R}_{r-1}^h, \tag{28}$$

$$\overrightarrow{W}_{n+1}^h = \overrightarrow{W}_3^h, \tag{29}$$

where $W^h$ is the variable of interest, $R^h$ is the source term, $r = 1, 2, 3$ is the number of stages, and the coefficients $\alpha_r$ are given by $\alpha_1 = 1/2$, $\alpha_2 = 1/2$ and $\alpha_3 = 1$.

# 6 NUMERICAL RESULTS

A code in Fortran90 was developed for the solution of Eq. (20), Eq. (21) and Eq.(24).

## 6.1 Problem with exact solution

To validate the computational code, we will consider that the exact solution of Eq. (7) and Eq. (8) is given by

$$\begin{aligned} u^1 &= \sin(t)\sin(\pi x)\sin(\pi y) \\ u^2 &= \sin(t)\cos(\pi x)\cos(\pi y) \\ p &= \sin(t)\left(\sin(\pi x) + \cos(\pi y) - \frac{2}{\pi}\right) \end{aligned}$$

in domain $\Omega = (0,1)^2$, a unit square. The source term $S_u$, the initial condition $u_0$ and the boundary conditions are obtained from $(u^1, u^2, p)$, which are solutions of the equations Eq. (7) and Eq. (8) for $\rho = 1$ and $\mu = 1$.

We show the reliability of the computer code through convergence rates. Note that we are working with P2/P1 element, thus velocity convergence expected rate is two (Layton, 2008), but the supreme norm is always able to estimate one further degree of convergence. From the interpolation theory $\|u - u_h\|_\infty = O(h^{k+1})$, where $k$ is the degree of basis function.

In Table 5 numerical error and convergence rates are analyzed. The smaller is the increment of the mesh, the smaller is the numerical error, i.e., adding degrees of freedom, the numerical solution approaches the exact solution. Moreover, expected convergence rates were obtained for velocity, since we used quadratic interpolation function (P2).

**Table 5: Numerical errors and convergence rates**

| h | $\|u - u^h\|_\infty$ | Rate | $\|\nabla(u - u^h)\|_{L^2}$ | Rate |
|---|---|---|---|---|
| 1/4 | 4.14e-3 | - | 1.04e-1 | - |
| 1/16 | 7.03e-5 | 2.940 | 6.28e-3 | 2.023 |
| 1/36 | 6.21e-6 | 2.992 | 1.23e-3 | 2.006 |

## 6.2 Fuel Cell

The Fig. 3(a) shows the contour lines of velocity, for ethanol flow rate of 1.0 ml min$^{-1}$ and pressure of $p = 1$ bar at the anode. The flow is laminar in all layers of the cell, with a velocity decrease from the end of the input channel up to the beginning the output channel. The fluid follows a parabolic profile in practically all channel. Fig. 3(b) shows a expanded view of the contour lines at the end of the diffusion layer and at the beginning of the output channel, with velocity vectors for better visualization of the flow direction.

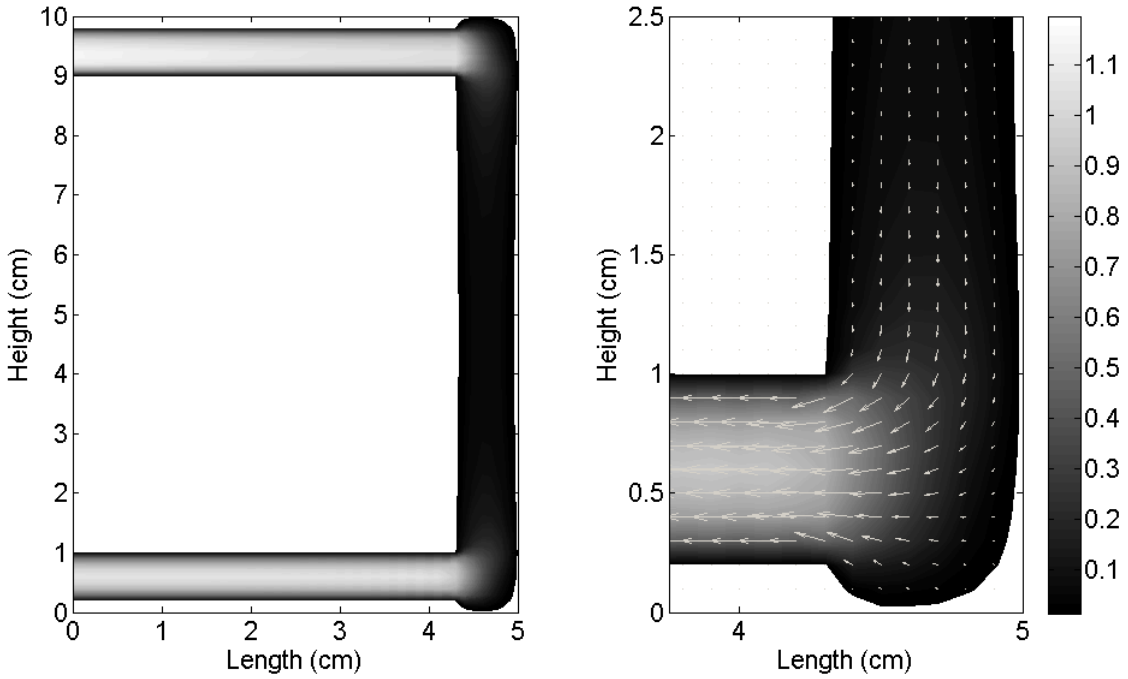


(a) Contour lines. (b) Zoom.

**Figure 3: Velocity contour lines inside the cell (anode side).**

Figure 4 shows the mole fraction of ethanol and water for two different current density values. The ethanol and water react to form the product carbon dioxide. These results show that the diffusion layer contributes to resistance of the total mass transfer. The mole fraction of ethanol and water remain constant along of the input channel, and decreases in the diffusion layer and on the catalyst surface.

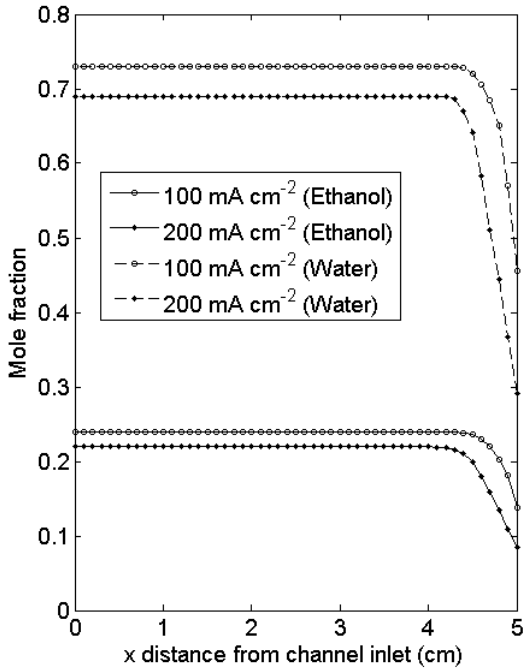


**Figure 4: Mole fraction of ethanol and water for cell temperature of 363 K, ethanol feed concentration of 1 M, and ethanol flow rate of 1.0 ml min$^{-1}$.**

Finally, the Fig. 5 shows the current density versus cell voltage for feed of 1 M ethanol concentration for two cell temperatures at the anode and cathode. In the first test case is considered the temperature of 315K at the anode and cathode and in the second case the temperature is 363K at the anode and 333K at the cathode. Fig. 5 shows the cell voltage increase with increasing temperature for given values of current density. In addition, it is seen that simulation results are in good agreement with experimental data given by Pramanik and Basu (2010). Note that the greater the current density the lowest is the cell voltage, for the conditions investigated in this work. This loss of cell voltage is due to activation overpotential, ohmic losses and concentration overpotentials, as discussed in section 4.

# 7 CONCLUSIONS

In this work, it was developed a two-dimensional model for direct ethanol fuel cells. The reactive flow was solved based on the Navier-Stokes equations for the flow, and for the mass fraction of each species, considering losses overpotentials for anode and cathode sides. Obtained results are in agreement with experimental data found in the literature for two different cell temperatures. The finite element method proved to be a good for solving the flow and

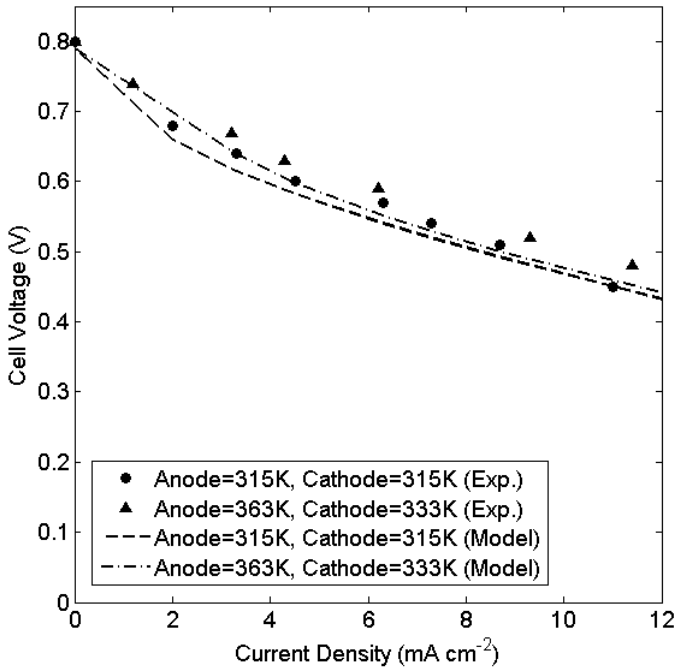


**Figure 5: Current density versus cell voltage for two cell temperatures and 1 M ethanol concentration.**

the equations of the species. As most of the work found in the literature is focused on one-dimensional fuel cell models, this work contributes with the development of a two-dimensional mathematical model for direct ethanol fuel cells considering all losses. Moreover, it is shown the mole fraction variations for ethanol and water in front of the membrane, what is not frequently found in the literature.

# REFERENCES

Abdullah, S, Kamarudin, S.K., Hasran, U.A., Masdar, M.S. & Daud, W.R.W., 2014. Modeling and simulation of a direct ethanol fuel cell: An overview, *Journal of Power Sources*, vol. 262, pp. 401-406.

Abdullah, S, Kamarudin, S.K., Hasran, U.A., Masdar, M.S. & Daud, W.R.W., 2015. Development of a conceptual design model of a direct ethanol fuel cell (DEFC), *International Journal of Hydrogen Energy*, vol. 40, n. 35, pp. 11943-11948.

Al-Baghdadi, M.A., 2005. Modeling of proton exchange membrane fuel cell performance based on semi-empirical equations, *Renewable Energy*, vol. 30, n. 10, pp. 1587-1599.

Andreadis, G. & Tsiakaras, P., 2006. Ethanol crossover and direct ethanol PEM fuel cell performance modeling and experimental validation, *Chemical Engineering Science*, vol. 61, n. 22, pp. 7497-7508.

Andreadis, G., Podias, A.K.M. & Tsiakaras, P., 2008. The effect of the parasitic current on the direct ethanol PEM fuel cell operation, *Journal of Power Sources*, vol. 181, n. 2, pp. 214-227.

Bard, A.J. & Faulkner, L.R., 2001. *Electrochemical methods: fundamentals and applications*, Wiley: New York, ed. 2.

Brenner, S.C. & Scott, R., 2008. *The mathematical theory of finite element methods*, Springer-Verlag, New York.

Cheddie, D.F. & Munroe, N.D.H., 2006. Three dimensional modeling of high temperature PEM fuel cells, *Journal of Power Sources*, vol. 160, n. 1, pp. 215-223.

Colmati, F., Antolini, E & Gonzalez, E.R., 2006. Effect of temperature on the mechanism of ethanol oxidation on carbon supported Pt, PtRu and Pt3Sn electrocatalysts, *Journal of Power Sources*, vol. 157, n. 1, pp. 98-103.

Farhat, Z.N, 2004. Modeling of catalyst layer micro structural refinement and catalyst utilization in a PEM fuel cell, *Journal of Power Sources*, vol. 138, n. 1, pp. 68-78.

Futerko, P. & Hsing, I-M, 2000. Two-dimensional finite-element method study of the resistance of membranes in polymer electrolyte fuel cells, *Electrochimica Acta*, vol. 45, n. 11, pp. 1741-1751.

Ge, J. & Liu, H., 2007. A three-dimensional two-phase flow model for a liquid-fed direct methanol fuel cell, *Journal of Power Sources*, vol. 163, n. 2, pp. 907-915.

Goel, J. & Basu, S., 2015. Mathematical modeling and experimental validation of direct ethanol fuel cell, *International Journal of Hydrogen Energy*, vol. 40, n. 41, pp. 14405-14415.

Heysiattalab, S. & Shakeri, M., 2011. 2D analytical model for direct ethanol fuel cell performance prediction, *Smart Grid and Renewable Energy*, vol. 2, n. 4, pp. 427-433.

Johnson, C., 1987. *Numerical solution of partial differential equations by the finite element method*, Dover Publications.

Kareemulla, D. & Jayanti, S., 2009. Comprehensive one-dimensional, semi-analytical, mathematical model for liquid-feed polymer electrolyte membrane direct methanol fuel cells, *Journal of Power Sources*, vol. 188, n. 2, pp. 367-378.

Layton, W.J., 2008. *Introduction to the numerical analysis of incompressible viscous flows*, Society for Industrial and Applied Mathematics.

Liu, W. & Wang, C.-Y., 2007. Three-dimensional simulations of liquid feed direct methanol fuel cells, *Journal of the Electrochemical Society*, vol. 154, n. 3, pp. B352-B361.

Memming, R. & Bahnemann, D., 2015. *Semiconductor electrochemistry*. John Wiley & Sons.

Pramanik, H. & Basu, S., 2010. Modeling and experimental validation of overpotentials of a direct ethanol fuel cell, *Chemical Engineering and Processing: Process Intensification*, vol. 49, n. 7, pp. 635-642.

Suresh, N.S. & Jayanti, S., 2011. Cross-over and performance modeling of liquid-feed polymer electrolyte membrane direct ethanol fuel cells, *International Journal of Hydrogen Energy*, vol. 36, n. 22, pp. 14648-14658.

Yuan, X.-Z. R., Song, C., Wang, H. & Zhang, J., 2009. *Electrochemical impedance spectroscopy in PEM fuel cells: fundamentals and applications*, Springer Science & Business Media.